IEEE Photonics Journal
An IEEE Photonics Society Publication

Open Access

Moving Target Tracking and Imaging Through Scattering Media via Speckle-Difference-Combined Bispectrum Analysis

Volume 11, Number 6, December 2019

Yingbo Wang
Jie Cao
Chengqiang Xu
Yang Cheng
Xuemin Cheng
Qun Hao

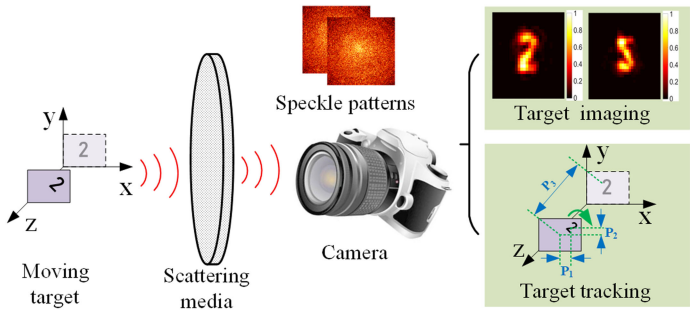

DOI: 10.1109/JPHOT.2019.2944934

Moving Target Tracking and Imaging Through Scattering Media via Speckle-Difference-Combined Bispectrum Analysis

Yingbo Wang,[1] Jie Cao,[1] Chengqiang Xu,[1] Yang Cheng,[1] Xuemin Cheng,[2] and Qun Hao [1]

[1]School of Optics and Photonics, Beijing Institute of Technology, Key Laboratory of Biomimetic Robots and Systems, Ministry of Education, Beijing 100081, China
[2]Graduate School at Shenzhen, Department of Precision Instrument, Tsinghua University, Shenzhen 518055, China

DOI:10.1109/JPHOT.2019.2944934

Manuscript received August 28, 2019; revised September 25, 2019; accepted September 28, 2019. Date of publication October 1, 2019; date of current version October 31, 2019. This work was supported in part by the National Natural Science Foundation of China (NSFC) under 61875012 and 61871031; in part by the Natural Science Foundation of Beijing Municipality under Grant 4182058; in part by Shanghai Space Science and Technology Innovation Fund SAST2017-083; in part by Shenzhen Science and Technology Innovation Program JCYJ20170412171011187; and in part by Graduate Technological Innovation Project of Beijing Institute of Technology 2019CX20027. Corresponding authors: Jie Cao and Qun Hao (email: ajieanyyn@163.com; qhao@bit.edu.cn).

Abstract: Target tracking and imaging through scattering media are challenges that must be overcome for important applications in various fields. The fundamental problem is the randomly diffused light in scattering media that prevents the formation of diffraction-limited images. In recent years, speckle correlation has emerged as a powerful approach for restoring targets through scattering media and tracking targets with high scattering. However, this method fails to achieve high-accuracy target tracking in multidimensional motion. Furthermore, retrieving the deterministic phase of a target in a low-resolution speckle pattern is limited. Here, a method based on speckle-difference-combined bispectrum analysis (SDCBA) is presented to simultaneously track and image targets. The proposed SDCBA requires no high-resolution pattern, randomly assigned initial values, nor numerous iterations. The target is tracked simultaneously in multidimension by using speckle difference autocorrelation and restored with the deterministic phase via bispectrum analysis of the low-resolution speckle pattern. This work carries out simulations and experiments to demonstrate simultaneous multidimensional target tracking and imaging in low-resolution speckle pattern through scattering media via the SDCBA. This work will benefit various fields, including biomedical applications, materials science, and military security.

Index Terms: Imaging through turbid media, speckle imaging, computation imaging, turbid media.

1. Introduction

Target tracking and imaging through scattering media by using speckle correlations have caught the attention of experts due to their wide applications in the biomedical field, materials science, and military security. Studies on target tracking and imaging have been conducted in the past few years; we summarize them from two aspects, namely, target tracking and imaging.

For target tracking through scattering media, Gariepy *et al.* [1] reported a solution that can locate hidden objects and track their motion using a femtosecond laser and a single-photon avalanche diode camera. However, this method fails to satisfy the demands of detecting and tracking small targets due to the inaccurate time measurement of laser ranging. Akhlaghi *et al.* [2] proposed a method that can track target motion via statistical analysis of integrated light using the full 3D trajectory of an object encoded by the temporal and spatial characteristics of a field. However, target tracking presents complexity as the temporal and spatial characteristics of a field must be measured every time a target is located in different scenarios. Chengfei *et al.* [3] proposed speckle correlation to realize target tracking without complex operation and optical setup in the presence of scattering media. However, this method proves ineffective in high-accuracy target tracking in a multi-dimension due to the influence of cross-correlation operation when the target is simultaneously moving in the multi-dimension direction.

For target imaging through scattering media, Vellekoop *et al.* [4] proposed a wavefront-shaping technique (WST) to focus light through a scattering medium via optical phase conjugation using a spatial light modulator (SLM) or digital micromirror device. Youngwoon *et al.* [5] experimentally demonstrated that the imaging capability of the WST overcomes the diffraction limit through scattering media. Subsequently, experts [6]–[9] further developed WST-based imaging and focusing techniques through scattering media. However, the drawback of invasive reference targets (i.e., guide star or known target) used [10], [11] and the low efficiency of feedback control mechanism limit imaging or focusing [12], [13]. Bertolotti *et al.* [14] proposed the scanning-based speckle correlation method, in which non-invasive imaging through scattering media is realized by the optical memory effect (OME) [15], [16] of the scattering media; however, the imaging speed is limited due to the low efficiency of data acquisition of scanning processes. Katz *et al.* [17] demonstrated a single-shot speckle correlation method that retrieves objects hidden behind the scattering layers using the autocorrelation of a single high-resolution speckle pattern via iterative phase retrieval algorithms [18]–[20]. However, this technique uses an iterative phase retrieval algorithm, resulting in the undetermined phase direction due to the randomly assigned initial values and inaccurate phase information caused by local minimum convergence. This technique also requires a high-resolution speckle pattern because it is based on the idea of using a statistical average [18], [21]. Tengfei *et al.* [21] experimentally demonstrated a single-shot noninvasive imaging scheme to realize diffraction-limited observation of hidden objects behind scattering layers without using iterative phase retrieval algorithms. However, this method requires a high-resolution speckle pattern to restrain the background noise [22].

To summarize, speckle correlation is a typical method for simultaneous target tracking and imaging through scattering media. However, target tracking and imaging feature two main drawbacks. On the one hand, speckle correlation fails to achieve simultaneous high-accuracy target tracking in multidimensional motion. On the other hand, this method requires a high-resolution speckle pattern.

Here, we report an effective noninvasive imaging method on the basis of speckle-difference-combined bispectrum analysis (SDCBA) to simultaneously solve the abovementioned issues. The core ideas of our method include simultaneous target tracking in a multidimension based on speckle difference and target restoration with the deterministic phase based on bispectrum analysis of low-resolution speckle patterns. Our method offers three advantages. (1) The moving target can be tracked accurately in multidimensional motion by using the autocorrelation of speckle difference. (2) The moving target can be restored by using low-resolution speckle patterns, whereas the target direction is determined using SDCBA. (3) Moving target tracking and imaging can be performed simultaneously without multiple iterations.

2. Theoretical Analysis

SDCBA involves three processes. First, the Fourier amplitude of a moving target is extracted via speckle difference, and the target is simultaneously tracked. Second, the Fourier phase is calculated using bispectrum analysis and the phase retrieval algorithm. Finally, the complex amplitude is formed using Fourier amplitude and Fourier phase, and the target is restored by the inverse Fourier

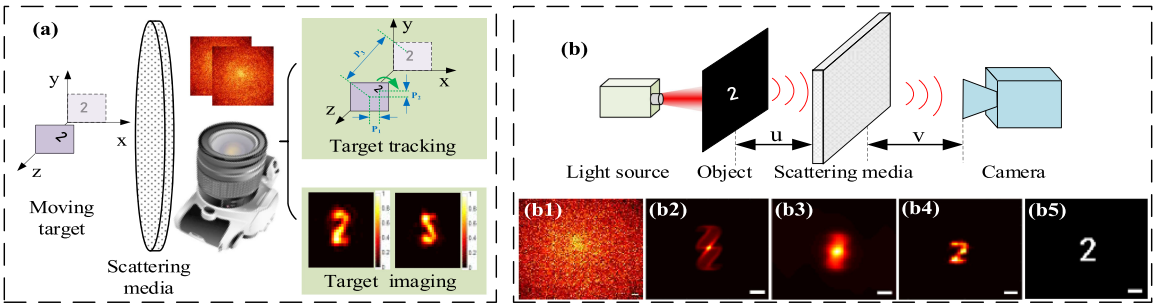

Fig. 1. Target tracking and imaging through scattering media. (a) Schematic of target tracking and imaging via SDCBA. (b) Schematic of target imaging via speckle correlation; (b1) raw speckle pattern; (b2) autocorrelation of the original target; (b3) autocorrelation of the raw speckle pattern; (b4) reconstructive target of speckle pattern; (b5) target used for imaging. Scale bars: 256 pixels in (b1) and 25 pixels in (b2), (b3), (b4), and (b5).

transform (IFFT) of complex amplitude. Fig 1(a) shows the schematic of target tracking and imaging through scattering media via SDCBA.

2.1 Target Tracking Via Speckle Difference

Speckle correlation function describes the relationship between OME and incident angle of light source. The correlation function of an incident angle can be written as follows:

$$C(\Delta\theta, \lambda, L) = \frac{\left(\frac{2\pi}{\lambda} \cdot \Delta\theta \cdot L\right)^2}{\left[\sinh\left(\frac{2\pi}{\lambda} \cdot \Delta\theta \cdot L\right)\right]^2}, \tag{1}$$

where $C(\Delta\theta, \lambda, L)$ refers to the relevancy of angle variables, λ denotes the wavelength, $\Delta\theta$ represents the angular difference of incident light, and L corresponds to the thickness of scattering media. In Eq. (1), when $C \geq 0.5$, the target is considered to travel within the memory-effect region [15].

Fig. 1(b) shows the schematic of target imaging through scattering media via speckle correlation. The target is illuminated using a pseudo-thermal light source. According to the OME theory, the speckle imaging process indicates the convolution of the point-spread-function (PSF) and target [18]. Imaging through scattering media can be computed as follows:

$$I(x) = \int_{-\infty}^{\infty} O(x)S(x - \delta x)dx + B = O(x) * S(x) + B, \tag{2}$$

where $*$ specifies the convolution, $I_{(x)}$ and $O_{(x)}$ denote the speckle and target patterns, respectively, $S_{(x)}$ stands for the PSF of optical system, x refers to the vector of spatial coordinates, and B is system noise. In scattering, the target can be viewed as a combination of numerous random point light sources. The speckle pattern in camera can be viewed as the superposition of all random speckle patterns when the target is illuminated by the incoherent light source [3], [17]. The autocorrelation of speckle intensity can be written as follows:

$$[I \star I](x) = [(O * S) \star (O * S)](x) = [(O \star O) * (S \star S)](x) = (O \star O) + C, \tag{3}$$

where $\star$ represents the correlation operator, C is an additional constant background term when the autocorrelation of the speckle pattern is a sharply peaked function [14], [23], and $S_n(x) \star S_n(x) \approx \delta(x)$. Eq. (3) proves the equivalency between the autocorrelations of the speckle pattern and target. Figs 1(b2) and 1(b3) show the autocorrelations of the target and a speckle pattern, respectively. The Wiener–Khinchin theorem suggests that the autocorrelation of speckle intensity is an equality with the Fourier transform (FT) of speckle power spectrum:

$$FT\{I * I\} = |FT\{I\}|^2, \tag{4}$$

where $FT\{\cdot\}$ is the FT operator. After removing the constant background term C, Fourier amplitude is obtained from Eq. (4), and Fourier phase (Fienup [24], *et al.*) is calculated to restore the target, as shown in Fig. 1(b4).

The speckle intensity of a moving target is captured by a camera and expressed by the equation below:

$$I(x+\Delta x) = O(x+\Delta x) * S(x+\Delta x) + B. \tag{5}$$

From Eqs. (2) and (5), the speckle difference of two frame speckle intensities before and after target movement is computed as follows:

$$\Delta I = I(x+\Delta x) - I(x) = O(x+\Delta x) * S(x+\Delta x) - O(x) * S(x), \tag{6}$$

where the target moves in the range of OME, $S(x+\Delta x) = S(x)$. The state after target movement is expressed as follows:

$$\Delta I \star \Delta I - O(x) \star O(x) = O(x+\Delta x) \star O(x+\Delta x) - [O(x) \star O(x+\Delta x)] - [O(x+\Delta x) \star O(x)], \tag{7}$$

Eq. (7) calculates the autocorrelation of speckle difference, whereas $O(x) \star O(x)$ can be calculated using Eq. (3). The first term on the right side of Eq. (7) refers to the autocorrelation of a moving target located at the center of the output plane. The last two items on the right side of Eq. (7) are the cross-correlations before and after target movement. The cross-correlation before and after target movement exhibits a symmetric pattern for the autocorrelation of target movement. The distance between the central part of cross-correlation and autocorrelation is Δx, $\Delta x = \Delta P \cdot A$, where ΔP is the number of pixels offset between autocorrelation and cross-correlation, and A is the pixel size of the camera.

When the target moves in the range of OME in the x–y plane, the distance of moving target in accordance with the pixels that are offset in the autocorrelation diagram can be written as follows:

$$\Delta x' = \frac{\Delta x \cdot u}{v} = \frac{\Delta P \cdot A \cdot u}{v}, \tag{8}$$

where u denotes the distance between the target and scattering media (i.e., object distance), and v refers to the distance between the scattering media and camera (i.e., image distance). Similarly, the pixel number of the reconstructive target should be set to N, and the size of reconstructive target is expressed as $y = \Delta N \cdot A \cdot u/v$.

Owing to the target tracking through speckle difference autocorrelation is based on the optical memory effect, the decorrelation size of scattering media should be calculated before target tracking. Only the range of the target movement fall into the range of optical memory effect, target tracking can be realized by our proposed method.

According to the analysis above, we carry out simulation on the basis of the speckle difference of two speckle patterns before and after target movement. Fig. 2 illustrates target tracking in the x–y plane.

Fig. 2 shows the simulation results of target tracking in the x–y plane. The target size and direction of target movement can be determined using Figs. 2(a4)–2(a6) due to the size of target autocorrelation is twice that of the target [25]. Fig. 2(b2) shows that the target shifts by 36 pixels along the x direction, consistent with the actual distance. Figs. 2(c2) and 2(c3) reveal that the target shifts by 36 and 31 pixels along the x and y directions, respectively, consistent with the actual target movement. In Fig. 2(d), rotational angle is determined via the Pearson correlation coefficient [10], which is computed as follows:

$$\rho_{X,Y} = \frac{\sum_{i=1}^{n}(X_i - \bar{X})(Y_i - \bar{Y})}{\sqrt{\sum_{i=1}^{n}(X_i - \bar{X})^2 \sum_{i=1}^{n}(Y_i - \bar{Y})^2}}, \tag{9}$$

where X denotes the autocorrelation of speckle pattern, Y represents the autocorrelation after target movement, $\bar{X}$ and $\bar{Y}$ are the mean values of X and Y, respectively. Fig. 2(d) shows that the target shifts by 36 pixels along the x direction and rotates 45° clockwise with respect to the z direction.

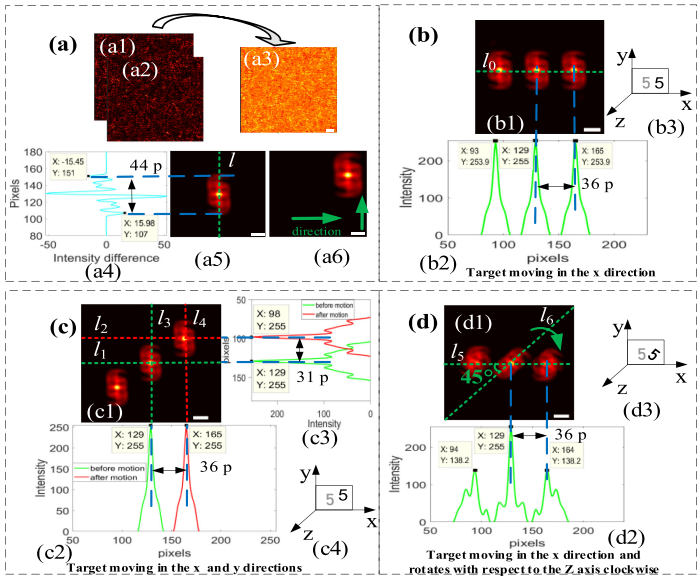

Fig. 2. Target tracking in the x–y plane. (a) Schematic of target tracking. (a1): Reference pattern (2048×2048) before target movement; (a2): speckle pattern (2048×2048) after target movement; (a3): speckle difference between (a1) and (a2); (a4): intensity difference curve of I in (a5); (a5) and (a6): autocorrelation of (a1) and (a2), respectively. (b) Target tracking in the x direction. (b1): Autocorrelation of speckle difference; (b2): intensity curve of I_0 in (b1); (b3): relative position before and after target movement. (c) Target tracking in the x and y directions. (c2): Green and red lines denote the intensity curves of I_1 and I_2, respectively; (c3): Green and red lines denote the intensity difference curves between adjacent pixels of I_3 and I_4, respectively. (d) Target tracking in the x direction with 45°clockwise rotation with respect to the z direction. (d1) and (d2) are similar to their counterparts in Fig. 2(b). Scale bars: 256 pixels in (a3) and 25 pixels in (a5), (a6), (b1), (c1), and (d1).

When the target moves in the range of OME along the z direction, and the camera is stationary, the imaging size of the moving target varies with object distance. The relationship between the zooming ratio of the imaging system, imaging size, autocorrelation size, and object distance can be expressed as follows:

$$\frac{\beta_1}{\beta_2} = \frac{p_1}{p_2} = \frac{c_1}{c_2} = \frac{u_2}{u_1}, \tag{10}$$

where β_1 and β_2 denote the zooming ratio of the imaging system when the target is located at u and $u + \Delta u$, respectively. p_1 and p_2 denote the imaging size, and c_1 and c_2 are the autocorrelation size. u_1 and u_2 are object distances.

Fig. 3(a) shows target tracking along the z direction. Comparing Fig. 2(a4) with Fig. 3(a1), the autocorrelation size of the target decreases from 44 pixels to 31 pixels due to the shift in target motion along the z direction. Therefore, the target displacement in the z direction can be calculated in accordance with Eq. (10). As shown in Fig. 3(b2) and 3(b3), the autocorrelation size after target movement and displacement in the x direction are 31 and 36 pixels, respectively, when the target moves in the x–z direction and rotates 45°anticlockwise. As observed from this section, the target moving in 4D (x–y–z direction and rotation) can be simultaneously tracked through speckle difference autocorrelation. The Fourier amplitude of a moving target can be obtained by performing a FT on the central part of the speckle difference autocorrelation.

2.2 Target Imaging Technique Through SDCBA

In the processes of target imaging through scattering media, the conventional imaging methods, speckle correlation and bispectrum analysis, requiring a high-resolution speckle pattern to obtain high image quality given that these methods are based on the idea of statistic average. Our proposed

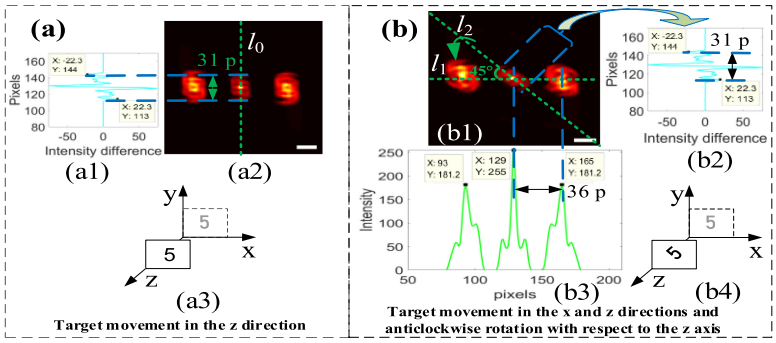

Fig. 3. Target tracking along the z direction. (a) Target tracking in the z direction only. (a1) Intensity difference curve of l_0 in Fig. 3(a2). (b) Target tracking in the z direction and 45°anticlockwise rotation with respect to the z axis. Scale bars: 25 pixels in (a2) and (b1).

method combines the advantages of speckle correlation and bispectrum analysis. The bispectrum analysis is used to provide the initial Fourier phase for the target Fourier phase extraction of the speckle correlation method. Because only the initial value in the iterative processes of the speckle correlation method needs to be generated, the initial Fourier phase with deterministic phase can be generated by the bispectrum analysis in a low-resolution speckle pattern. The initial Fourier phase can be used as the initial value of the phase extraction processes of speckle correlation method, then the Fourier phase of the target can be extracted by the speckle correlation method in a low-resolution speckle pattern. Our proposed method reduces the number of iterations in the phase extraction processes and facilitates convergence to the minimum. After the Fourier phase and Fourier amplitude of the target are obtained, the target can be reconstructed by the SDCBA method in a low-resolution speckle pattern. Fig. 4 shows the SDCBA flowchart.

The concrete steps of the SDCBA method are described as follows:

① The speckle difference pattern is calculated by the subtraction of two frame speckle patterns before and after target movement.

② The speckle difference autocorrelation is calculated using the correlation operation, and the central part of autocorrelation is obtained to calculate the Fourier amplitude.

③ The Fourier amplitude of the moving target is calculated by using the FT of the central part of the speckle difference autocorrelation.

④ The initial phase is calculated via bispectrum analysis of a speckle pattern after target movement, and the Fourier phase after target movement is calculated by the phase retrieval (i.e., GS) algorithm.

⑤ The target is restored by the IFFT of complex amplitude.

When the speckle pattern of a moving target is obtained, it can be divided into multiple sub-speckles. Each sub-speckle is expressed as the convolution of a target and the corresponding sub-PSF. The overall average of all sub-speckle bispectra is expressed by the following:

$$\left\langle B_{I_s}\right\rangle_N = B_o \cdot \left\langle B_{p_s}\right\rangle_N, \tag{11}$$

where $\langle B\rangle$ represents the average operator of B, n refers to the number of sub-images, B is the bispectrum, I_s corresponds to the sub-speckle, o is the target, and p_s is the sub-PSF. Given that the spatially averaged bispectrum of the whole sub-PSF approximates real values [21], [26], the phase information of speckle bispectrum is consistent with that of the target bispectrum, and the relationship can be written as follows:

$$\arg\{\left\langle B_{I_s}\right\rangle_N\} \approx arg\{B_o\}. \tag{12}$$

Considering that the phase information of a target bispectrum contains the Fourier phase information of the target, the Fourier phase information of a target can be expressed as follows:

$$\phi_{-u_1-u_2} = \arg\{\left\langle B_{I_s}\right\rangle_N\} - \phi_{u_1} - \phi_{u_2}, \tag{13}$$

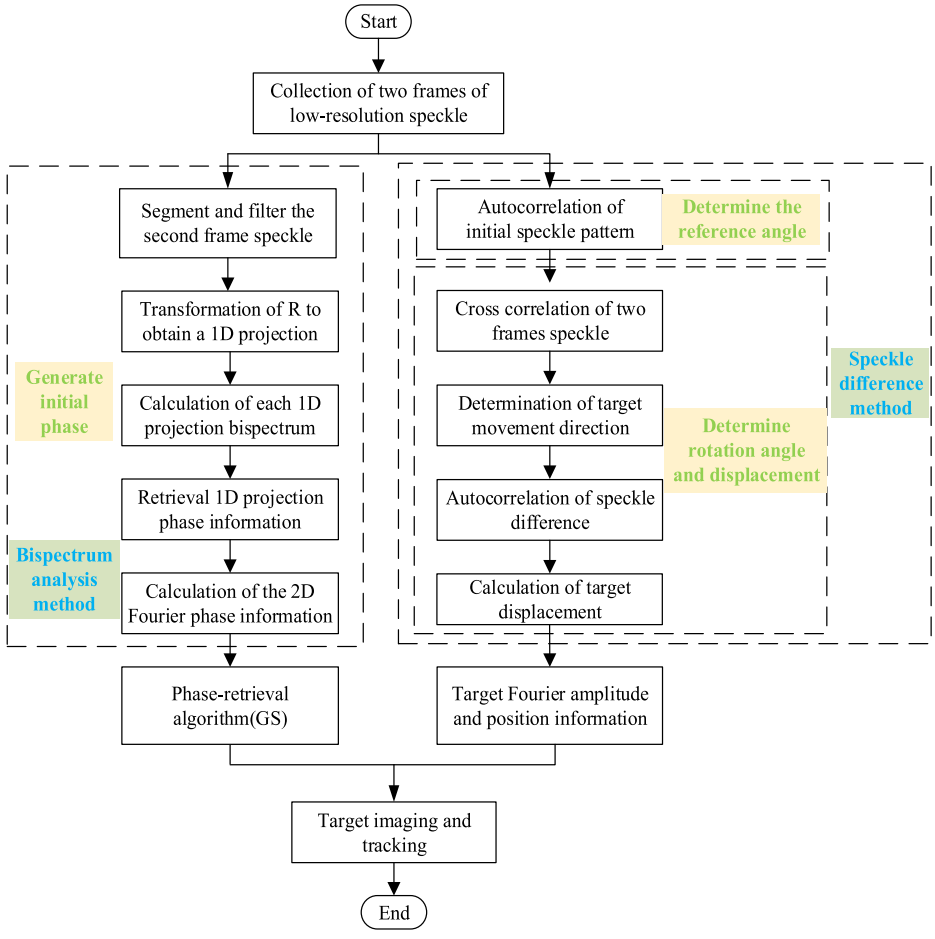

Fig. 4. SDCBA flowchart.

where φ_{u1} and φ_{u2} denote the Fourier phases of different frequencies. Given that the target is tracked via the speckle difference autocorrelation, we only need to restore the structural information of the target rather than its specific location. Therefore, we assume the initial condition as $\varphi_0 = \varphi_1 = 0$, and the high frequencies can be obtained using recursive algorithm. In accordance with the Fourier central slice theorem, the 1D Fourier phase is arranged in a certain position by using the projection angle of the 2D Fourier space [21], [27]. The coordinate system transformation is completed by converting the polar coordinate system into a Cartesian coordinate system. The initial Fourier phase of the target is obtained by arranging all the recovered 1D Fourier phases according to their corresponding positions. The complete Fourier phase of a moving target is calculated using the Gerchberg–Saxton (GS) algorithm. The GS algorithm starts with an initial guess for the target pattern $g_1(x, y)$ and selects the result of bispectrum analysis. This initial guess is entered the algorithm, which performs the following steps at kth iteration:

$$\begin{cases} G_k(k_x, k_y) = FT\{g_k(x, y)\} \\ \theta_k(k_x, k_y) = \arg\{G_k(k_x, k_y)\} \\ G'_k(k_x, k_y) = \sqrt{S_{meas}(k_x, k_y)}e^{i\theta_k(k_x, k_y)}, \\ g'_k(k_x, k_y) = FT^{-1}\{G'_k(k_x, k_y)\} \end{cases} \tag{14}$$

where $S_{\text{meas}}(\cdot)$ is the power spectrum of target image, that is, $S_{\text{meas}}(k_x, k_y) = |FT\{O(x, y)\}|^2$. The input for the next $(k+1)$ iteration, $g_{k+1}(x, y)$, is obtained from the output of kth iteration, $g'_k(x, y)$, by

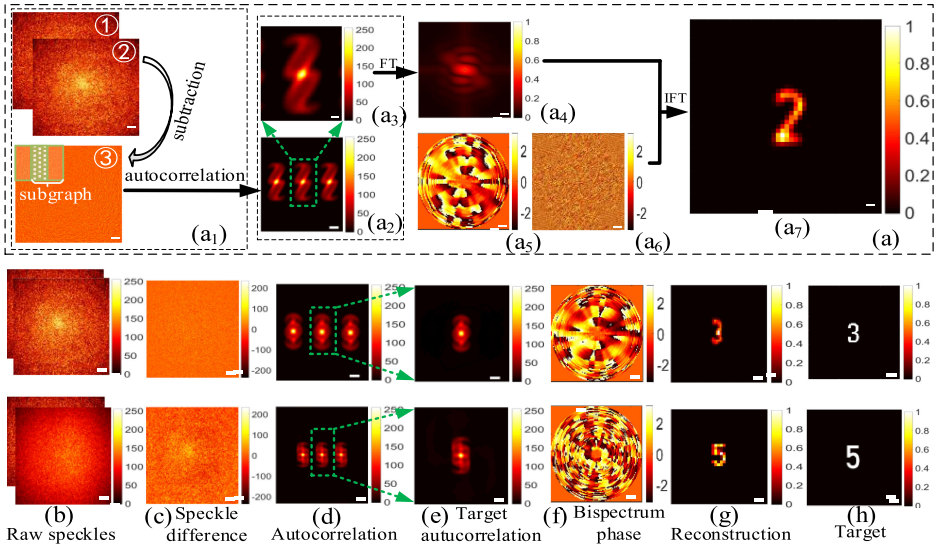

Fig. 5. Schematic of target imaging and comparison of imaging results. Scale bars: 256 pixels in (a1), (b), and (c) and 25 pixels in (a2)–(a6) and (d)–(h).

imposing physical constraints on the target image as real and non-negative in our implementation [17]. The "Hybrid Input-Output (HIO)" and "Error reduction (ER)" are used to form the "ER-HIO" algorithm for the physical constraints. The "ER-HIO" algorithm is described as follows:

$$g_{k+1}(x, y) = \begin{cases} g_k(x, y) & (x, y) \notin \Gamma \\ g_k(x, y) - \beta g'_k(x, y) & (x, y) \in \Gamma \end{cases}, \tag{15}$$

where Γ denotes the set of all points (x, y) on $g'_k(x, y)$ violating the physical constraints, and β refers to a feedback parameter that determines the performance of the convergency of algorithm. When the Fourier phase of a target is obtained from Eq. (14), the moving target can be restored by combining with the Fourier amplitude of the target from Eq. (4).

Fig. 5(a) shows the imaging processes of SDCBA. As shown in Fig. 5(a7), the digit "2" is recovered from the speckle pattern by the SDCBA method. In Fig. 5, the last two rows represent the simulated imaging results of moving targets, digits "3" and "5", hidden behind the scattering media. The moving targets are restored realistically, and desirable results are obtained as shown in Figs. 5(g) and 5(h).

3. Experimental Setup and Results

3.1 Target Tracking and Imaging Through Scattering Media in Transmissive Experiment

Experiments are carried out to verify the capability of target tracking and imaging with SDCBA. Figs. 6(a) and 6(b) display the schematic and experimental setup, respectively. The target is a letter "F", which is filtered from a negative United States Air Force resolution target (1951 USAF, Thorlabs). The target is illuminated using a narrow-bandwidth LED source with 625 nm central wavelength (M625L4, Thorlabs). The scattering medium is a ground glass diffuser (DG100 $\times$ 100-220, Thorlabs) positioned 40 cm away from the target. The translation stage (GCM-910403M, Daheng Optics) that can shift in 4D (x–y–z direction and rotation) is used to control target movement. The speckle intensity patterns are captured using a camera (MV-SUA630C/M, Mind Vision, 2.4 μm pixel size). The camera is hidden 5 cm behind the scattering media, and a narrowband filter is fixed in front of the camera to obtain a high-contrast speckle pattern. An iris of suitable aperture is placed behind the ground glass diffuser to determine the resolution of reconstructive target.

The target is moved manually during experiments, and the speckle patterns of moving target are captured using a camera. To quantify the accuracy of target tracking, the target is continuously

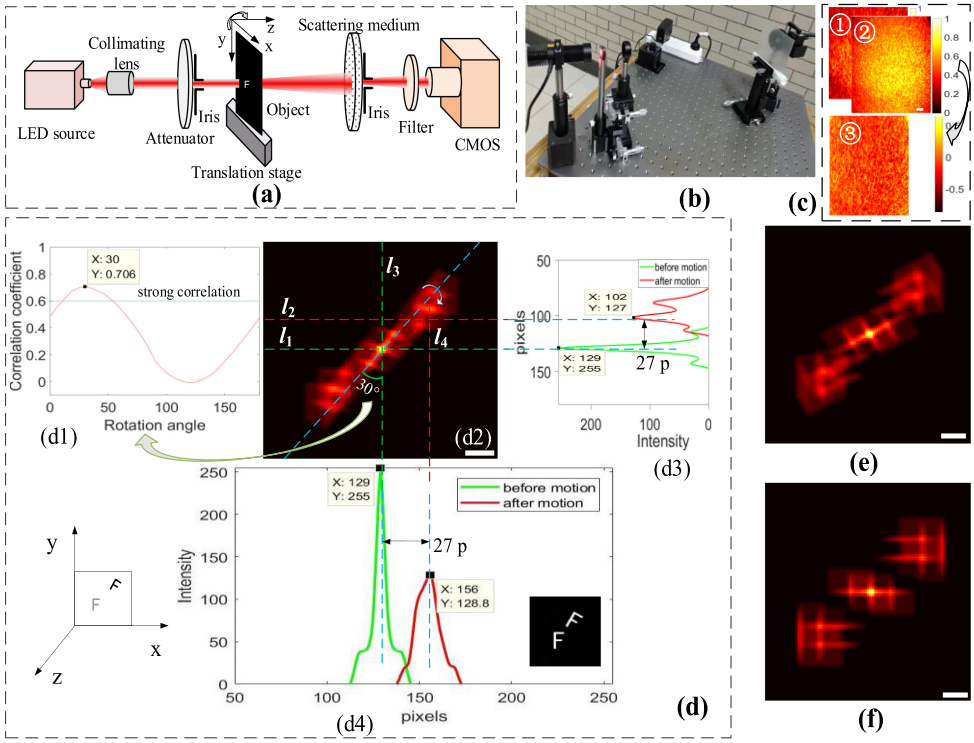

Fig. 6. Schematic of transmissive experiment and the experimental results of target tracking in 3D (x–y and rotation). (a) Schematic of target tracking and imaging through scattering media in transmissive experiment; (b) experimental setup for tracking and imaging hidden moving target; (c) raw speckle patterns and speckle-difference diagram; (d) detailed processes of target tracking in the 3D plane direction (the target moves by 0.5 mm in x and y direction and rotates 30°clockwise with respect to the z direction). (d1): Relationship between the rotational angles and correlation coefficients in accordance with Eq. (9); (d2): autocorrelation of speckle difference before and after target movement in the 3D plane direction; (e), (f) autocorrelation of speckle difference (x, y: 1 mm movement, 60°rotation; x, y: 1.5 mm movement, 90°rotation); Scale bars: 256 pixels in (c) and 25 pixels in (d2), (e), and (f).

moved for three times. The target is consistently moved 0.5 mm away from the former position in the x and y directions and simultaneously rotated 30°clockwise with respect to the z direction every time. Here, we mainly explain the target tracking experiments result in the first movement phase. Figs. 6(c)–6(f) summarize the experimental results of target tracking in 3D (x–y direction and rotation). Fig. 6(d1) shows that the target rotates by 30°with respect to the z direction, consistent with the actual rotational angle of the target. Similar to the analysis of Figs. 2(c2) and 2(c3), Figs. 6(d3) and 6(d4) show that the target shifts by 27 pixels in the x and y direction, respectively. The displacement of moving target equals 0.518 mm according to Eq. (8) and is close to the actual displacement of the target (0.5 mm). Thus, measurement error is related to pixel size, object distance, and image distance.

In the other phases of target movement, the offset of ΔP pixels of the moving target in the x–y direction is calculated using the method in Fig. 2. The experimental results for the moving target are calculated in accordance with Eq. (8) as shown in column 4 of Table 1, and the experimental results $\Delta x'$ agree well with the actual values Δx. Table 1 shows that the relative error of target tracking reaches less than 4%, whereas the total relative error is less than 2%. The rotational angles of target are determined using Eq. (9) when the reference angle is changed by a step size of 1°. The angular accuracy of a moving target can be further improved when the step of reference angle is reduced.

Figs. 7(a)–7(d) summarize the experimental results of 4D target tracking and imaging. The target is continuously moved thrice in the experiments. Fig. 7(b) shows the detailed processes of target

TABLE 1
Experimental Results and Actual Values With target "F" in the 3D Direction (x–y Direction and Rotation)

Moving direction	Actual values Δx /mm	Pixels offset ΔP	Experimental results $\Delta x'$/mm	Relative error	Total displacement /mm	Total relative error
x direction	0.5	27	0.518	**3.6%**	1.516	**1.067%**
	0.5	26	0.499	0.2%		
	0.5	26	0.499	0.2%		
y direction	0.5	27	0.518	**3.6%**	1.516	**1.067%**
	0.5	26	0.499	0.2%		
	0.5	26	0.499	0.2%		
Rotation (°)	30°	—	30°	0	89°	**1.11%**
	30°	—	29°	**3.3%**		
	30°	—	30°	0		

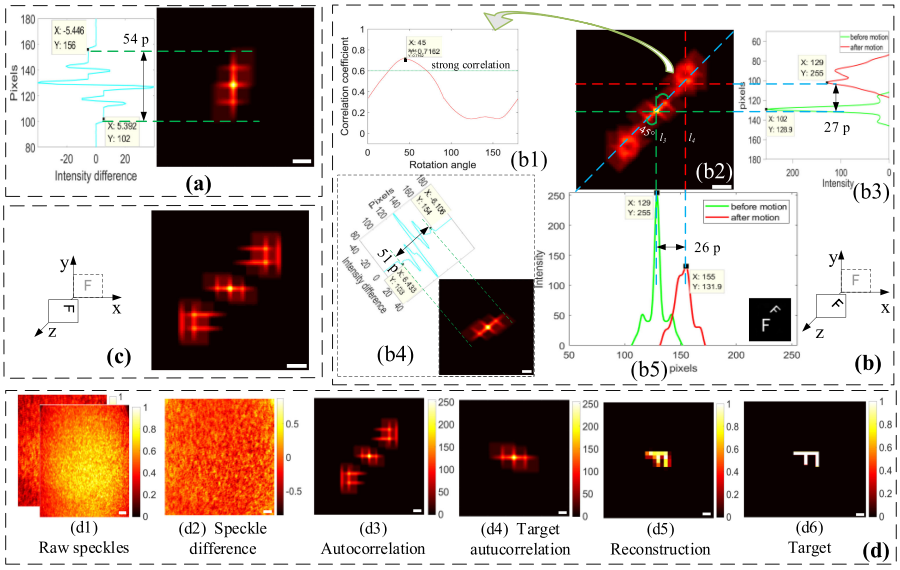

Fig. 7. Experimental results of target tracking and imaging in 4D (x–y–z direction and rotation). (a) Autocorrelation size before target movement; (b) detailed processes of target tracking in the z direction. (b1): Relationship between rotational angles and correlation coefficients. (b2): Autocorrelation of speckle difference. (b3) and (b5): Displacement in the x–y direction similar to those in Figs. 6(d3) and 6(d4), respectively. (b4): Autocorrelation size after target movement. (c) Autocorrelation of speckle difference in the third state. (d) Imaging processes after target movement. (i.e., 1.5 mm in x–y direction, 3 cm in the z direction, and at 90°clockwise rotation with respect to the z direction); Scale bars: 256 pixels in (d1) and (d2) and 25 pixels in (a)–(c) and (d3)–(d6).

tracking in the second state, in which the target is continuously moved 0.5 mm in the x–y direction and 1 cm in the z direction (object distance: 42 cm) and rotated 45° clockwise with respect to the z direction. Fig. 7(b1) shows the 45° rotational angle at the maximum correlation coefficient. Figs. 7(b3) and 7(b5) show that the target shifts by 26 and 27 pixels in the x and y direction respectively, and the 0.499 mm and 0.518 mm displacement calculated using Eq. (2). The autocorrelation size after target movement totals 51 pixels as shown in Fig. 7(b4). Thus, displacement in the z direction spans 42.35 cm according to Eq. (10). Table 2 shows the experimental results of the

TABLE 2
Experimental Results and Actual Values With Target "F" in the 4D Direction

Moving direction	Actual values Δx /mm	Pixels offset ΔP	Experimental results $\Delta x'$/mm	Relative error	Total /mm	Total relative error
x direction	0.5	27	0.518	3.6%	1.516	1.067%
	0.5	**26**	0.499	0.2%		
	0.5	26	0.499	0.2%		
y direction	0.5	26	0.499	0.2%	1.516	1.067%
	0.5	**27**	0.518	3.6%		
	0.5	26	0.499	0.2%		
z direction	41	1	40.75	0.610%	43.2	0.465%
(Object	**42**	**3**	42.35	0.833%		
distance/cm)	43	4	43.2	0.465%		
Rotation (°)	0°	—	0°	0	90°	—
	45°	—	45°	0		
	45°	—	45°	0		

three-time processing of target tracking, whereas the data in bold in Fig. 7(b) represent the tracking results of the second state. The relative error of target tracking reaches less than 4% in the x–y direction and less than 1% in the z direction. In comparison of the results in Table 1, the accuracy of target tracking in the x–y direction in the 3D state approximates that of the corresponding 4D state direction. Fig. 7(d) shows that the direction of reconstructive target is 90°relative to the initial direction of target, consistent with the direction following target movement.

3.2 Target Tracking and Imaging Through Scattering Media in Reflective Experiment

For practical applications, a reflective experiment is designed to verify the capability of tracking and imaging of hidden moving targets. In the experiments, a liquid crystal SLM with amplitude modulation only is used to load the target. A 1 mm target is loaded in the SLM; the distance between the SLM and ground glass diffuser is 40 cm. The SLM is illuminated by the same LED source, which is collimated using a lens with 2.5 cm focal length. The 45°polarizations of the two polarizers are selected before and after SLM to achieve the best contrast. The beam is reflected by the target on SLM, and it passes through the beam splitter and scattering medium. Speckle patterns are captured by the camera. The distance between the camera and ground glass diffuser is 8.5 cm, and the iris is fixed at the back of the ground glass diffuser to improve the space resolution of the reconstructive target. Figs. 8(a) and 8(b) show the schematic and experimental setup of target tracking and imaging through scattering media in reflective experiment, respectively.

In the reflective experiments, the target is loaded on different positions of SLM to simulate target movement, and SLM is fixed on an automatic translation stage for 4D movement. To simplify the experiment, we only simulate the target movement on the SLM plane. The moving targets, the digit "4" and letter "R", are separately loaded on the SLM and are moved by 0.5 mm in the x direction. The raw speckle patterns (2560 $\times$ 2560) are captured before and after target movement. The pixel offsets before and after target movement are calculated via the autocorrelation of speckle difference. The target shifts by 46 pixels as shown in Fig. 8(c3), and displacement (0.519 mm) of target movement is calculated in accordance with Eq. (8). The relative error of target tracking is less than 4%. Fig. 8(c7) shows that the targets are restored by the proposed method, and the reconstructed targets exhibit the clear outlines of a moving target.

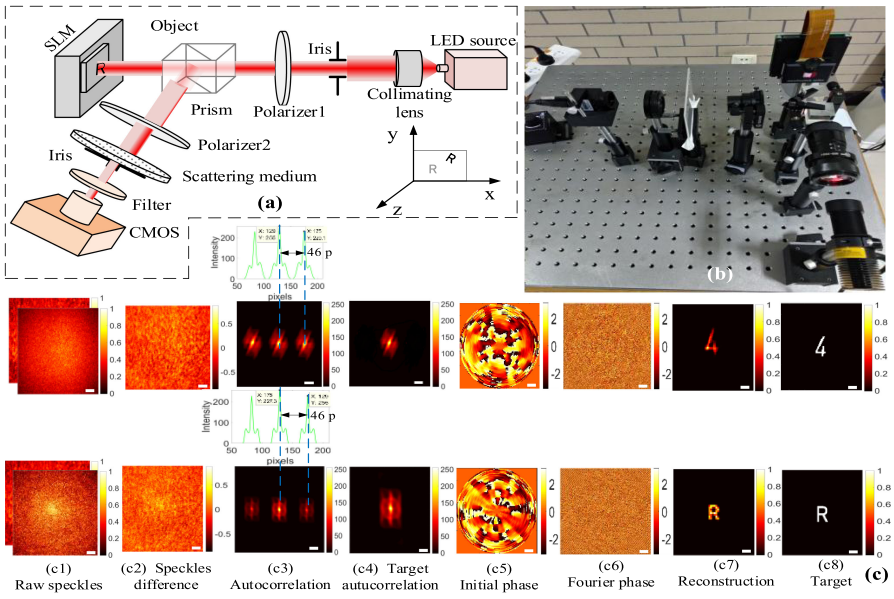

Fig. 8. Target tracking and imaging through scattering media in reflective experiment. (a) Schematic of tracking and imaging of hidden moving target in the reflective experiment; (b) experimental setup of a reflective experiment; (c) tracking and imaging of moving target. Scale bars: 256 pixels in (c1) and (c2) and 25 pixels in (c3)–(c8).

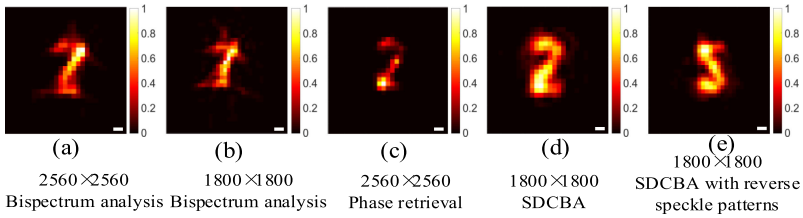

Fig. 9. Target imaging results of different methods. Scale bars: 256 pixels in (c1) and (c2) and 15 pixels in (c3)–(c8).

The imaging effect of SDCBA is compared with that of other methods. Fig. 9 shows the results of an extended experiment. The comparison methods of target imaging include bispectrum analysis with different resolutions, phase retrieval algorithm, and SDCBA. The different resolution speckle patterns captured by setting the region of interest of the camera. Figs. 9(a) and 9(b) show the results of target imaging through bispectrum analysis with 2560×2560 and 1800×1800 speckle resolutions, respectively. Fig. 9(c) shows the result of target imaging through phase retrieval algorithm, 60 iterations of "ER-HIO," β values ranging from 2 to 0, and a step size of 0.02. The imaging quality in Fig. 9(a) is better than that in Fig. 9(c) at the same resolution. Figs. 9(d) and 9(e) display the imaging results of our proposed SDCBA with low-resolution speckle patterns of different directions using 20 iterations of "ER-HIO," β values ranging from 2 to 0, and a step size of 0.02. Fig. 9(e) presents the reconstructed result of reversed speckle patterns. The target direction can be determined using SDCBA when the directional information of a target can be determined using bispectrum analysis. To further quantitatively evaluate the imaging quality of a target by using different methods, we introduce the mean square error (MSE), structural similarity (SSIM) index, and the time of target imaging. From Table 3, the SDCBA shows a better imaging quality than the other methods, but the real-time performance of the proposed method needs to be further improved. Computer hardware configuration: Windows 10 64 bit, CPU (i7-7700HQ @ 2.8 GHz), RAM (8 G, DDR42667MHz), MATLAB2017b.

TABLE 3
Quantitative Comparison of Results Obtained Using Different Imaging Methods

Target digit "2"	Bispectrum-analysis (2560×2560)	Bispectrum-analysis (1800×1800)	Phase retrieval (2560×2560)	SDCBA (1800×1800)
MSE	0.390	0.495	0.394	**0.379**
SSIM	0.802	0.758	0.779	**0.857**
Time (s)	95	40	12	**25**

4. Discussion

To further improve the tracking accuracy and imaging quality and considering practical applications, we discuss three factors that affect system performance.

First, for practical applications, there are two problems need to be solved, one is the optical memory angle should be expanded to accommodate large targets and range of motion; the other is the target tracking and imaging model should be optimized to improve the real-time performance of the algorithm. Target dimensions and range of motion should fall within the angular memory effect field of view, y $<<$ $u{\cdot}\lambda/(\pi{\cdot}L)$, and the axial extent of target should be within the axial decorrelation length, $\delta z << 2{\cdot}\lambda(u/D)^2/\pi$ [28], [29] as SDCBA depends on angular correlations inherent in scattering. Therefore, the thickness of scattering media should be reduced, and the distance between the target and scattering media should be increased to expand the optical memory angle. Meanwhile, a small iris radius is selected to expand the depth of axial movement of target. The multiple memory effect angles also can be jointed to expand the memory effect angle when the target be illuminated by using multiple light sources. In order to improve the real-time performance of target tracking and imaging, a new model should be established. For example, first obtaining the PSF of system, and then imaging through deconvolution method; first target imaging, and then target tracking through contour matching and so on.

Second, the velocity of target movement should be matched with the camera exposure time to improve the tracking accuracy for a moving target. At a certain camera pixel size (A), a clear target image is obtained when the velocity (v) and exposure time (Δt) satisfy the matching relationship, $v \bullet \Delta t \bullet \beta \leq A$. However, the accuracy of target tracking is reduced as the motion blur of an image is generated when the target is moving at high speed. Therefore, a high-frame-rate camera should be used in experiments to improve the accuracy of tracking moving targets at high speed.

Third, to improve the imaging quality of moving target, we should select the right light source and filter. A pseudo-thermal light source is ideal because it is produced by lasers that pass through a rotating frosted glass. However, the preparation of a pseudo-thermal light source presents complexity. Therefore, a LED light source with less than 10 nm bandwidth should be used to replace the pseudo-thermal light source. A narrow band filter with less than 1 nm bandwidth can be used to suppress stray light in experiments.

5. Conclusion

SDCBA is presented for target tracking and imaging through scattering media. The proposed method is analyzed and simulated, and the results are consistent with the actual values in target tracking and imaging. We successfully tracked and imaged the target through scattering media via SDCBA in transmissive and reflective experiments. The experimental results of target tracking show that the relative errors of plane and axial tracking are less than 4% and less than 1%, respectively. The moving target hidden behind the scattering media is restored via SDCBA of low-resolution speckle patterns, and the direction is determined simultaneously. SDCBA features a higher SSIM index and lower MSE than the other methods used. Aside from tracking and imaging of binary-amplitude targets, if select a narrow-bandwidth illumination and suppress the system background light, our method can also be extended to tracking and imaging of gray-scale targets. Our imaging

technique is scalable as it utilizes the angular memory effect [29]. Given the appropriate optimization, our method features potential application for biomedical imaging, bioscience, and military security.

Acknowledgment

The authors would like to thank Y. Li for useful discussion of the experiment.

References

[1] G. Gariepy *et al.*, "Detection and tracking of moving objects hidden from view," *Nature Photon.*, vol. 10, no. 1, pp. 23–26, 2016.
[2] M. I. Akhlaghi and D. Aristide, "Tracking hidden objects using stochastic probing," *Optica*, vol. 4, no. 4, pp. 447–453, 2017.
[3] C. Guo, J. Liu, T. Wu, L. Zhu, and X. Shao, "Tracking moving targets behind a scattering medium via speckle correlation," *Appl. Opt.*, vol. 57, no. 4, pp. 905–913, 2018.
[4] I. M. Vellekoop and A. P. Mosk, "Focusing coherent light through opaque strongly scattering media," *Opt. Lett.*, vol. 32, no. 16, pp. 2309–2311, 2007.
[5] C. Youngwoon *et al.*, "Overcoming the diffraction limit using multiple light scattering in a highly disordered medium," *Phys. Rev. Lett.*, vol. 107, no. 2, pp. 23902–23905, 2011.
[6] S. Kang *et al.*, "High-resolution adaptive optical imaging within thick scattering media using closed-loop accumulation of single scattering," *Nature Commun.*, vol. 8, no. 1, 2017, Art. no. 2157.
[7] X. Tao, T. Lam, B. Zhu, Q. Li, M. R. Reinig, and K. Joel, "Three-dimensional focusing through scattering media using conjugate adaptive optics with remote focusing (CAORF)," *Opt. Exp.*, vol. 25, no. 9, pp. 10368–10383, 2017.
[8] I. M. Vellekoop, A. Lagendijk, and A. P. Mosk, "Exploiting disorder for perfect focusing," *Nature Photon.*, vol. 4, no. 5, pp. 320–322, 2010.
[9] M. Cui, "Parallel wavefront optimization method for focusing light through random scattering media," *Opt. Lett.*, vol. 36, no. 6, pp. 870–872, 2011.
[10] H. He, Y. Guan, and J. Zhou, "Image restoration through thin turbid layers by correlation with a known object," *Opt. Exp.*, vol. 21, no. 10, pp. 12539–12545, 2013.
[11] D. Akbulut, T. J. Huisman, E. G. Putten, Van, W. L. Vos, and A. P. Mosk, "Focusing light through random photonic media by binary amplitude modulation," *Opt. Exp.*, vol. 19, no. 5, pp. 4017–4029, 2011.
[12] O. Katz, E. Small, and Y. Silberberg, "Looking around corners and through thin turbid layers in real time with scattered incoherent light," *Nature Photon.*, vol. 6, no. 8, pp. 549–553, 2012.
[13] T. Peng *et al.*, "Real-time optical manipulation of particles through turbid media," *Opt. Exp.*, vol. 27, no. 4, pp. 4858–4866, 2019.
[14] J. Bertolotti, E. G. Van Putten, C. Blum, A. Lagendijk, W. L. Vos, and A. P. Mosk, "Non-invasive imaging through opaque scattering layers," *Nature*, vol. 491, no. 7423, pp. 232–234, 2015.
[15] I. I. Freund, M. Rosenbluh, and S. Feng, "Memory effects in propagation of optical waves through disordered media," *Phys. Rev. Lett.*, vol. 61, no. 20, pp. 2328–2331, 1988.
[16] S. Feng, C. Kane, P. A. Lee, and A. D. Stone, "Correlations and fluctuations of coherent wave transmission through disordered media," *Phys. Rev. Lett.*, vol. 61, no. 7, pp. 834–387, 1988.
[17] O. Katz, P. Heidmann, M. Fink, and S. Gigan, "Non-invasive single-shot imaging through scattering layers and around corners via speckle correlations," *Nature Photon.*, vol. 8, no. 10, pp. 784–790, 2014.
[18] J. R. Fienup, "Phase retrieval algorithms: A comparison," *Appl. Opt.*, vol. 21, no. 15, pp. 2758–2769, 1982.
[19] G. S. Manuel, S. T. Thurman, and J. R. Fienup, "Efficient subpixel image registration algorithms," *Opt. Lett.*, vol. 33, no. 2, pp. 156–158, 2008.
[20] Y. Shechtman, Y. C. Eldar, O. Cohen, H. N. Chapman, J. Miao, and M. Segev, "Phase retrieval with application to optical imaging," *IEEE Signal Process. Mag.*, vol. 32, no. 3, pp. 87–109, May 2015.
[21] W. Tengfei, K. Ori, S. Xiaopeng, and G. Sylvain, "Single-shot diffraction-limited imaging through scattering layers via bispectrum analysis," *Opt. Lett.*, vol. 41, no. 21, pp. 5003–5006, 2016.
[22] C. L. Nikias, "Bispectrum estimation: A digital signal processing framework," *Proc. IEEE*, vol. 75, no. 7, pp. 869–891, Jul. 1987.
[23] I. Freund, "Joseph W. Goodman: Speckle Phenomena in Optics: Theory and Applications," *J STAT PHYS*, vol. 130, no. 2, pp. 413–414, 2008.
[24] J. R. Fienup and C. C. Wackerman, "Phase-retrieval stagnation problems and solutions," *J. Opt. Soc. America A*, vol. 3, no. 11, pp. 1897–1907, 1986.
[25] S. E. Skipetrov, J. Peuser, R. Cerbino, P. Zakharov, B. Weber, and F. Scheffold, "Noise in laser speckle correlation and imaging techniques," *Opt. Exp.*, vol. 18, no. 14, pp. 14519–14534, 2010.
[26] A. W. Lohmann, G. Weigelt, and B. Wirnitzer, "Speckle masking in astronomy: Triple correlation theory and applications," *Appl. Opt.*, vol. 22, no. 24, pp. 4028–4037, 1983.
[27] P. A. Midgley and M. Weyland, "3D electron microscopy in the physical sciences: The development of Z-contrast and EFTEM tomography," *Ultramicroscopy*, vol. 96, no. 3, pp. 413–431, 2003.
[28] I. Freund, "Looking through walls and around corners," *Physica A Statistical Mechanics Appl.*, vol. 168, no. 1, pp. 49–65, 1990.
[29] M. Cua, E. H. Zhou, and C. Yang, "Imaging moving targets through scattering media," *Opt. Exp.*, vol. 25, no. 4, pp. 3935–3945, 2017.